

A Multivariate Regression Approach to Association Analysis of Quantitative Trait Network

Seyoung Kim Kyung-Ah Sohn Eric P. Xing

TECHNICAL REPORT
CMU-ML-08-113

School of Computer Science
Carnegie Mellon University
Pittsburgh, PA 15213

Abstract

Many complex disease syndromes such as asthma consist of a large number of highly related, rather than independent, clinical phenotypes, raising a new technical challenge in identifying genetic variations associated simultaneously with correlated traits. In this study, we propose a new statistical framework called graph-guided fused lasso (GFlasso) to address this issue in a principled way. Our approach explicitly represents the dependency structure among the quantitative traits as a network, and leverages this trait network to encode structured regularizations in a multivariate regression model over the genotypes and traits, so that the genetic markers that jointly influence subgroups of highly correlated traits can be detected with high sensitivity and specificity. While most of the traditional methods examined each phenotype independently and combined the results afterwards, our approach analyzes all of the traits jointly in a single statistical method, and borrow information across correlated phenotypes to discover the genetic markers that perturb a subset of correlated traits jointly rather than a single trait. Using simulated datasets based on the HapMap consortium data and an asthma dataset, we compare the performance of our method with the single-marker analysis, and other sparse regression methods such as the ridge regression and the lasso that do not use any structural information in the traits. Our results show that there is a significant advantage in detecting the true causal SNPs when we incorporate the correlation pattern in traits using our proposed methods.

Keywords: lasso, fused lasso, association analysis, quantitative trait network

1 Introduction

Recent advances in high-throughput genotyping technologies have significantly reduced the cost and time of genome-wide screening of individual genetic differences over millions of single nucleotide polymorphism (SNP) marker loci, shedding light to an era of “personalized genome” [1,

2]. Accompanying this trend, clinical and molecular phenotypes are being measured at phenome and transcriptome scale over a wide spectrum of diseases in various patient populations and laboratory models, creating an imminent need for appropriate methodology to identify omic-wide association between genetic markers and complex traits which are implicative of causal relationships between them. Many statistical approaches have been proposed to address various challenges in identifying genetic locus associated with the phenotype from a large set of markers, with the primary focus on problems involving a univariate trait [3, 4, 5]. However, in modern studies the patient cohorts are routinely surveyed with a large number of traits (from measures of hundreds of clinical phenotypes to genome-wide profiling of thousands of gene expressions), many of which are correlated among them. For example, in Figure 1, the correlation structure of the 53 clinical traits in the asthma dataset collected as a part of the Severe Asthma Research Program (SARP) [6] is represented as a network, with each trait as a node, the interaction between two traits as an edge, and the thickness of an edge representing the strength of correlation. Within this network, there exists several subnetworks involving a subset of traits, and furthermore, the large subnetwork on the left-hand side of Figure 1 contains two subgroups of densely connected traits with thick edges. In order to understand how genetic variations in asthma patients affect various asthma-related clinical traits in the presence of such a complex correlation pattern among phenotypes, it is necessary to consider all of the traits jointly and take into account their correlation structure in the association analysis. Although numerous research efforts have been devoted to studying the interaction patterns among many quantitative traits represented as networks [7, 8, 9, 10, 11, 12, 13, 14] as well as discovering network submodules from such networks [11, 15], this type of network structure has not been exploited in association mapping [16, 17]. Many of the previous approaches examined one phenotype at a time to localize the SNP markers with a significant association and combined the results from a set of such single-phenotype association mapping across phenotypes. However, we conjecture that one can detect additional weak associations and at the same time reduce false signals by combining the information across multiple phenotypes under a single statistical framework.

In QTL mapping studies with pedigree data, a number of approaches have been proposed to detect pleiotropic effect of markers on multiple correlated traits by considering the traits jointly. However, these approaches involve only a weak and indirect form of structural information present in the phenotypes. The methods based on multivariate regression [18, 19, 20] with multiple outcomes were concerned with finding genetic loci that influence all of the phenotypes jointly, rather than explicitly taking into account the complex interaction patterns among the phenotypes. A different approach has been proposed that first applies principle component analysis (PCA) to the phenotypes and uses the transformed phenotypes in a single-phenotype association test [21, 22]. The transformation via PCA allows to extract the components that explain the majority of variation in phenotypes, but has a limitation in that it is not obvious how to interpret the derived phenotypes.

More recently, in expression quantitative trait locus (eQTL) analysis with microarray gene expression measurements treated as quantitative traits, researchers have begun to combine an explicit representation of correlation structure in phenotypes, such as gene networks, with genotype information to search for genetic causes of perturbations of a subset of highly correlated phenotypes [23, 24, 25, 26]. A module network [11], which is a statistical model developed for un-

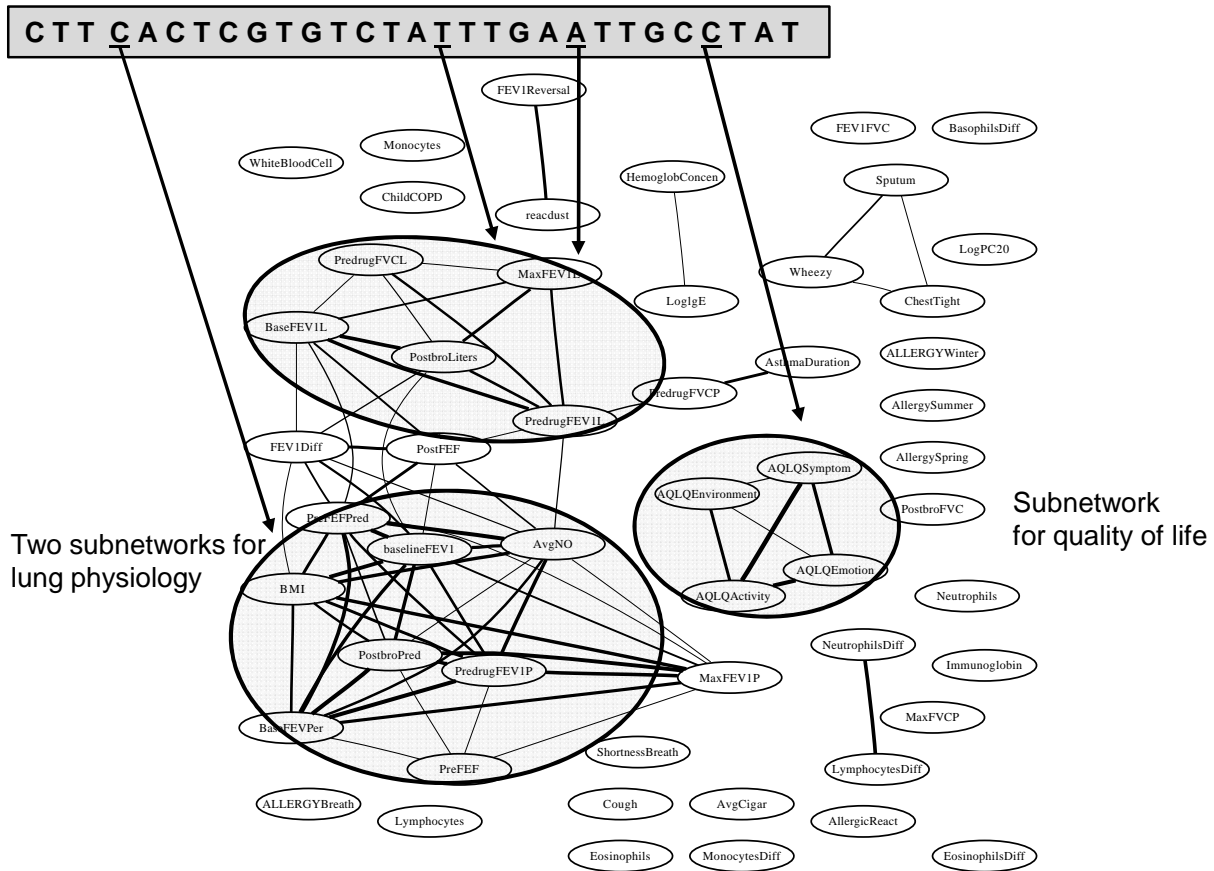


Figure 1: Illustration of association analysis using phenotype correlation graph for asthma dataset

covering regulatory modules from gene expression data, was extended to incorporate genotypes of regulators, such that the expression of genes regulated by the same regulator was explained by the variation of both the expression level and the genotype of the regulators [23]. Although the model was able to identify previously unknown genetic perturbations in yeast regulatory network, the genotype information used in the model was limited to markers in regulators rather than the whole genome. Several other studies incorporated a gene co-regulation network in a genome-wide scan for association. In a network eQTL association study for mouse [24], a gene co-regulation network was learned, a clustering algorithm was applied to this network to identify subgroups of genes whose members participate in the same molecular pathway or biological process, and then, a single-phenotype analysis was performed between genotypes and the phenotypes within each subgroup. If the majority of phenotypes in each subgroup were mapped to the common locus in the genome, that locus was declared to be significantly associated with the subgroup. Using this approach, new obesity-related genes in mouse were identified by examining the network module associated with the genetic locus previously associated with obesity-related traits such as body mass index and cholesterol level. A similar analysis was performed on yeast, where clusters of

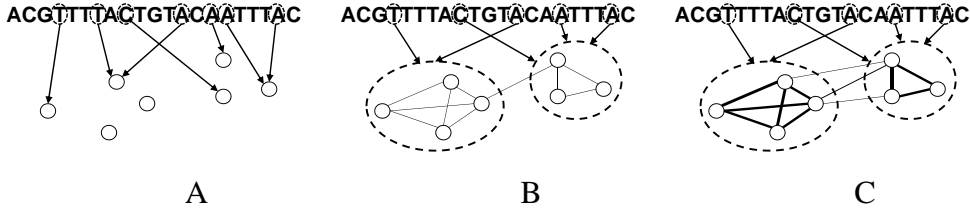


Figure 2: Illustrations for multiple output regression with A: lasso, B: graph-constrained fused lasso, and C: graph-weighted fused lasso.

yeast genes were mapped to a common eQTL hotspots [26]. One of the main disadvantages of this approach is that it first applies a clustering algorithm to identify subgroups of phenotypes in the network, rather than directly incorporating the network itself as a correlation structure, since the full network contains much richer information about complex interaction patterns than the clusters of phenotypes. Another disadvantage of this approach is that it relies on a set of single-phenotype statistical tests and combines the results afterwards in order to determine whether a marker is significantly affecting a subgroup of phenotypes, thus requiring a substantial effort in conducting appropriate multiple hypothesis testing. We believe that an approach that considers markers and all of the phenotypes jointly in a single statistical method has the potential to increase the power of detecting weak associations and reduce susceptibility to noise.

In this article, we propose a family of methods, called the *graph-guided fused lasso* (GFlasso), that fully incorporates the quantitative-trait network as an explicit representation for correlation structure without applying additional clustering algorithms to phenotypes. Our methods combine multiple phenotypes in a single statistical framework, and analyze them jointly to identify SNPs perturbing a subset of tightly correlated phenotypes instead of combining results from multiple single-phenotype analyses. The proposed methods leverage a dependency graph defined on multiple quantitative traits such as the graph for the asthma-related traits shown in Figure 1, assuming that such a graph structure is available from preprocessing steps or as prior knowledge from previous studies. It is reasonable to assume that when a subset of phenotypes are highly correlated, the densely connected subgraphs over these correlated traits contain variables that are more likely to be synergistically influenced by the same or heavily overlapping subset(s) of SNPs with similar strength than an arbitrary subset of phenotypes.

The proposed approach is based on a multivariate regression formalism with the L_1 penalty, commonly known as the lasso, that achieves “sparsistency” in the estimated model by setting many of the regression coefficients for irrelevant markers to zero [27, 28]. As a brief digression for clarity, sparsistency refers to an asymptotic property in high-dimensional statistical inference that for the estimator of a p -dimensional vector θ from n iid samples, where p can be $\gg n$, the probability of recovering the true non-zero elements $S = \{i : \theta_i \neq 0\}$ in the estimator approach one in the limit, if the true non-zero elements are sparse in the sense that $|S| \leq n \ll p$ [28]. This property of the lasso makes it a natural approach for genome wide association analysis, where the marker genotypes are treated as the predictors, the phenotype in question is treated as the response, and the (sparse) set of markers having non-zero regression coefficients are interpreted as

the markers truly associated with the phenotype. However, when applied to association mapping with multivariate traits, the lasso is equivalent to a single-trait analysis that needs to be repeated over every single trait. In other words, for a collection of traits, each trait would be treated as independent of all other traits, and every trait would be regressed on a common set of marker genotypes via its own lasso (Figure 2A), ignoring the possible coupling among traits. Our innovations in GFlasso that enable a departure from the baseline lasso for a single trait is that, in addition to the lasso penalty, we employ a “fusion penalty” that fuses regression coefficients across correlated phenotypes, using either unweighed or weighted connectivity of the phenotype graph as a guide. This additional penalty will encourage sharing of common predictors (i.e., associated markers) to coupled responses (i.e., traits). The two fusion schemes lead to two variants of the GFlasso: a *graph-constrained fused lasso* (G_c GFlasso) based on only the graph topology (Figure 2B), and a *graph-weighted fused lasso* (G_w GFlasso) that offers a flexible range of stringency of the graph constraints through edge weights (Figure 2C). We developed an efficient algorithm based on quadratic programming combined with gradient search for estimating the regression coefficients under GFlasso. The results on two datasets, one simulated from HapMap SNP markers and the other collected from asthma patients, show that our method outperforms competing algorithms in identifying markers that are associated with a correlated subset of phenotypes.

2 Material and Methods

2.1 Lasso Regression for Multiple Independent Phenotypes

Let \mathbf{X} be an $N \times J$ matrix of genotypes for N individuals and J SNPs, where each element x_{ij} of \mathbf{X} is assigned 0, 1, or 2 according to the number of minor alleles at the j -th locus of the i -th individual. Let \mathbf{Y} denote an $N \times K$ matrix of K quantitative trait measurements over the same set of individuals. We use \mathbf{y}_k to denote the k -th column of \mathbf{Y} . A conventional single-trait association via linear regression model can be applied to this multiple-trait setting by fitting the model to \mathbf{X} and each of the K traits \mathbf{y}_k ’s separately:

$$\mathbf{y}_k = \mathbf{X}\boldsymbol{\beta}_k + \boldsymbol{\epsilon}_k, \quad \forall k = 1, \dots, K, \quad (1)$$

where $\boldsymbol{\beta}_k$ is a J -vector of regression coefficients for the k -th trait that can be used in a statistical test to detect SNP markers with significant association, and $\boldsymbol{\epsilon}_k$ is a vector of N independent error terms with mean 0 and a constant variance. We center each column of \mathbf{X} and \mathbf{Y} such that $\sum_i y_{ik} = 0$ and $\sum_i x_{ij} = 0$, and consider the model in Equation (1) without an intercept. We obtain the estimates of $\mathbf{B} = \{\boldsymbol{\beta}_1, \dots, \boldsymbol{\beta}_K\}$ by minimizing the residual sum of squares:

$$\hat{\mathbf{B}} = \operatorname{argmin} \sum_k (\mathbf{y}_k - \mathbf{X}\boldsymbol{\beta}_k)^T \cdot (\mathbf{y}_k - \mathbf{X}\boldsymbol{\beta}_k). \quad (2)$$

In a typical genome-wide association mapping, one examines a large number of marker loci with the goal of identifying the region associated with the phenotypes and markers in that region. A straight-forward application of the linear regression method in Equation (2) to association mapping

with large J can cause several problems such as an unstable estimate of regression coefficients and a poor interpretability due to many irrelevant markers with non-zero regression coefficients. Sparse regression methods such as forward stepwise selection [29], ridge regression [30, 5], and lasso [27] that select a subset of markers with true association have been proposed to handle the situation with large J . Forward stepwise selection method iteratively selects one relevant marker at a time while trying to improve the model fit based on Equation (2), but it may not produce an optimal solution because of the greedy nature of the algorithm. Ridge regression has an advantage of performing the selection in a continuous space by penalizing the residual sum of square in Equation (2) with the L_2 norm of β_k 's and shrinking the regression coefficients toward zero, but it does not set the regression coefficients of irrelevant markers to exactly zero. We use the lasso that penalizes the residual sum of square with the L_1 norm of regression coefficients and has the property of setting regression coefficients with weak association markers exactly to zero, thus offering the advantages of both forward stepwise selection and ridge regression. The lasso estimate of the regression coefficients can be obtained by solving the following:

$$\hat{\mathbf{B}}^{\text{lasso}} = \underset{\mathbf{B}}{\text{argmin}} \sum_k (\mathbf{y}_k - \mathbf{X}\beta_k)^T \cdot (\mathbf{y}_k - \mathbf{X}\beta_k) + \lambda \sum_{k,j} |\beta_{kj}| \quad (3)$$

where λ is a regularization parameter that controls the amount of sparsity in the estimated regression coefficients. Setting λ to a large value increases the amount of penalization, setting more regression coefficients to zero. Many fast algorithms are available for solving Equation (3) [27, 31].

The lasso for multiple-trait association mapping in Equation (3) is equivalent to solving a set of K independent regressions for each trait with its own L_1 penalty, and does not provide a mechanism to combine information across multiple traits such that the estimates reflect the potential relatedness in the regression coefficients for those correlated traits that are influenced by common SNPs. However, several traits are often highly correlated such as in gene expression of co-regulated genes in eQTL study, and there might be genotype markers that are jointly associated with those correlated traits. Below, we extend the standard lasso and propose a new penalized regression method for detecting markers with pleiotropic effect on correlated quantitative traits.

2.2 Graph-Guided Fused Lasso for Multiple Correlated Phenotypes

In order to identify markers that are predictive of multiple phenotypes jointly, we represent the correlation structure over the set of K traits as an edge-weighted graph, and use this graph to guide the estimation process of the regression coefficients within the lasso framework. We assume that we have available from a pre-processing step a phenotype correlation graph G consisting of a set of nodes V , each representing one of the K traits, and a set of edges E . In this article, we adopt a simple and commonly-used approach for learning such graphs, where we first compute pairwise Pearson correlation coefficients for all pairs of phenotypes using \mathbf{y}_k 's, and then connect two nodes with an edge if their correlation coefficient is above the given threshold ρ . We set the weight of each edge $(m, l) \in E$ to the absolute value of correlation coefficient $|r_{m,l}|$, so that the edge weight represents the strength of correlation between the two nodes. This thresholded correlation graph is also known as a relevance network, and has been widely used as a representation of gene

interaction networks [32, 33]. It is worth pointing out that the choice of methods for obtaining the phenotype network is not a central issue of our method. Other variations of the standard relevance network have been suggested [34], and any of these graphs can also be used within our proposed regression methods. Below, we first introduce G_c Flasso that makes use of unweighted graph, and further extend this method to G_w Flasso to take into account the full information in the graph including edge weights.

Given the correlation graph of phenotypes, it is reasonable to assume that if two traits are highly correlated and connected with an edge in the graph, their variation across individuals might be explained by genetic variations at the same loci, possibly having the same amount of influence on each trait. In G_c Flasso, this assumption is expressed as an additional penalty term that fuses two regression coefficients β_{jm} and β_{jl} for each marker j if traits m and l are connected with an edge in the graph, as follows:

$$\hat{\mathbf{B}}^{\text{GC}} = \underset{\mathbf{B}}{\text{argmin}} \sum_k (\mathbf{y}_k - \mathbf{X}\boldsymbol{\beta}_k)^T \cdot (\mathbf{y}_k - \mathbf{X}\boldsymbol{\beta}_k) + \lambda \sum_k \sum_j |\beta_{jk}| + \gamma \sum_{(m,l) \in E} \sum_j |\beta_{jm} - \text{sign}(r_{ml})\beta_{jl}|, \quad (4)$$

where λ and γ are regularization parameters that determine the amount of penalization. The last term in Equation (4) is called a fusion penalty [35], and encourages β_{jm} and $\text{sign}(r_{m,l})\beta_{jl}$ to take the same value by shrinking the difference between them toward zero. A larger value for γ leads to a greater fusion effect, or greater sparsity in $|\beta_{jm} - \text{sign}(r_{m,l})\beta_{jl}|$'s. We assume that if two traits m and l connected with an edge in G are negatively correlated with $r_{ml} < 0$, the effect of a common marker on those traits takes an opposite direction, and we fuse β_{jm} and $(-\beta_{jl})$, or equivalently, β_{jm} and $\text{sign}(r_{m,l})\beta_{jl}$. When the fusion penalty is combined with the lasso penalty as in Equation (4), the lasso penalty sets many of the regression coefficients to zero, and for the remaining non-zero regression coefficients, the fusion penalty flattens the values across multiple highly correlated phenotypes for each marker so that the strength of influence of each marker becomes similar across those correlated traits. The idea of fusion penalty has been first used in the classical regression problem over univariate response (i.e., single-output) from high-dimensional covariates to fuse the regression coefficients of two adjacent covariates when the covariates are assumed to be ordered such as in time [35]. This corresponds to coupling pairs of elements in the adjacent rows of the same column in the coefficient matrix \mathbf{B} in Equation (4). In G_c Flasso, we employ a similar strategy in a multiple-output regression in order to identify pleiotropic effect of markers, and let the trait correlation graph determine which pairs of regression coefficients should be fused. Now, every such coupled coefficient pair corresponds to the elements of the corresponding two columns in the same row of matrix \mathbf{B} in Equation (4). It is possible to show the asymptotic properties of estimators of the GFlasso methods as $N \rightarrow \infty$ analogous to the ones previously shown for the lasso and the fused lasso [35, 36].

In a multiple-trait association mapping, networks of clinical traits or molecular traits (i.e., gene expressions) typically contain many subnetworks within which nodes are densely connected, and we are interested in finding the genetic variants that perturb the entire set of traits in each subnetwork. This can potentially increase the power of detecting weak associations between genotype

and phenotype that may be missed when each phenotype is considered independently. When used in this setting, the $G_c\text{Flasso}$ looks for associations between a genetic marker and a subgraph of phenotype network rather than a single phenotype. Unlike other previous approaches for detecting pleiotropic effect that first apply clustering algorithms to learn subgroups of traits and then search for genetic variations that perturb the subgroup, $G_c\text{Flasso}$ uses the full information on correlation structure in phenotypes available as a graph, where the subgroup information is embedded implicitly within the graph as densely connected subgraphs. Although the fusion penalty in the $G_c\text{Flasso}$ is applied locally to a pair of regression coefficients for neighboring trait pairs in the graph, this fusion effect propagates to the regression coefficients for other traits that are connected to them in the graph. For densely connected nodes, the fusion is effectively applied to all of the members of the subgroup, and the set of non-zero regression coefficients tend to show a block structure with the same values across the correlated traits given a genotype marker with pleiotropic effect on those traits, as we demonstrate in experiments. If the edge connections are sparse within a group of nodes, the corresponding traits are only weakly related, and there is little propagation of fusion effect through edges in the subgroup. Thus, the $G_c\text{Flasso}$ incorporates the subgrouping information through the trait correlation graph in a more flexible manner compared to previous approaches.

Now, we present a further generalization of $G_c\text{Flasso}$ that exploit the full information in the phenotype networks for association mapping. Note that the only structural information used in the $G_c\text{Flasso}$ is the presence or absence of edges between two phenotypes in the graph. The $G_w\text{Flasso}$ is a natural extension of the $G_c\text{Flasso}$ that takes into account the edge weights in graph G in addition to the graph topology. The $G_w\text{Flasso}$ weights each term in the fusion penalty in Equation (4) by the amount of correlation between the two phenotypes being fused, so that the amount of correlation controls the amount of fusion. More generally, $G_w\text{Flasso}$ weights each term in the fusion constraint in Equation (4) with a monotonically increasing function of the absolute values of correlations, and finds an estimate of the regression coefficients as follows:

$$\begin{aligned} \hat{\mathbf{B}}^{\text{GW}} = \operatorname{argmin} & \sum_k (\mathbf{y}_k - \mathbf{X}\boldsymbol{\beta}_k)^T \cdot (\mathbf{y}_k - \mathbf{X}\boldsymbol{\beta}_k) \\ & + \lambda \sum_k \sum_j |\beta_{jk}| + \gamma \sum_{(m,l) \in E} f(r_{ml}) \sum_j |\beta_{jm} - \operatorname{sign}(r_{ml})\beta_{jl}|. \end{aligned} \quad (5)$$

If the two phenotypes m and l are highly correlated in graph G with a relatively large edge weight, the fusing effect increases between these two phenotypes since the difference between the two corresponding regression coefficients β_{jm} and β_{jl} is penalized more than for other pairs of phenotypes with weaker correlation. In this article, we consider $f_1(r) = |r|$ for $G_w^1\text{Flasso}$ and $f_2(r) = r^2$ for $G_w^2\text{Flasso}$. We note that the $G_c\text{Flasso}$ is a special case of the $G_w\text{Flasso}$ with $f(r) = 1$.

The optimization problems in Equations (4) and (5) can be formulated as a quadratic programming as described in Appendix, and there are many publicly available software packages that efficiently solve such quadratic programming problems. The regularization parameters λ and γ can be determined by a cross-validation or a validation set, although for a large problem, a grid search for the λ and γ can be time-consuming. In order to improve the efficiency in determining the λ and γ , we use a gradient-descent type of algorithm as described in Appendix.

2.3 Simulation Scheme for Model Validation

We simulated genotype data for 250 individuals based on the HapMap data in the region of 8.79-9.20M in chromosome 7. The first 60 individuals of the genotype data came from the parents of the HapMap CEU panel. We generated genotypes for additional 190 individuals by randomly mating the original 60 individuals on the CEU panel. We included only those SNPs with minor allele frequency greater than 0.1. Since our primary goal is to measure the performance of the association methods in the case of multiple correlated phenotypes, we sampled 50 SNPs randomly from the 697 SNPs in the region in order to reduce the correlation among SNPs from the linkage disequilibrium.

Given the simulated genotype, we generated the true associations represented as regression coefficients \mathbf{B} and phenotype data as follows. We assumed that the number of phenotypes is 10, and that there are three groups of correlated phenotypes of size 3, 3, and 4, respectively, so that the phenotypes in each group form a subnetwork in the correlation graph of phenotypes. We randomly selected three SNPs as affecting all of the phenotypes in the first subnetwork, and four SNPs as influencing each of the remaining two subnetwork. We assumed that there is one additional SNP affecting phenotypes in the first two subnetworks, which corresponds to the case of a SNP perturbing a super-network consisting of two subnetworks such as the large subnetwork on the left-hand side of Figure 1. In addition, we assumed one additional SNP affecting all of the phenotypes. We set the effect size of all of the true association SNPs to the same value. Once we set the regression coefficients according to this setup, we generated the phenotype data with noise distributed as $N(0, 1)$, using the simulated genotypes as covariates.

2.4 Asthma Dataset

We apply our methods to data collected from 543 asthma patients as a part of the Severe Asthma Research Program (SARP). The genotype data were obtained for 34 SNPs within or near IL-4R gene that spans a 40kb region on chromosome 16. This gene has been previously shown to be implicated in severe asthma [37]. We used the publicly available software *PHASE* [38] to impute missing alleles and phase the genotypes. The phenotype data included 53 clinical traits related to severe asthma such as age of onset, family history, and severity of various symptoms. The phenotype correlation graph thresholded at 0.7 as shown in Figure 1 reveals several subnetworks of correlated traits. For example, the subset of traits related to lung physiology (the nodes for baselineFEV1, PreFEFPred, PostbroPred, PredrugFEV1P, Max FEV1P, etc.) form a large subnetwork on the left-hand side of Figure 1, whereas traits representing quality of life of the patients (the nodes for AQLQ Environment, AQLQSymptom, AQLQ Emotion, and AQLQ Activity) are found in a small subnetwork near the center of Figure 1. Our goal is to examine whether any of the SNPs in the IL-4R gene are associated with a subnetwork of correlated traits rather than an individual trait. We standardized measurements for each phenotype to have mean 0 and standard deviation 1 so that their values are roughly in the same range across phenotypes.

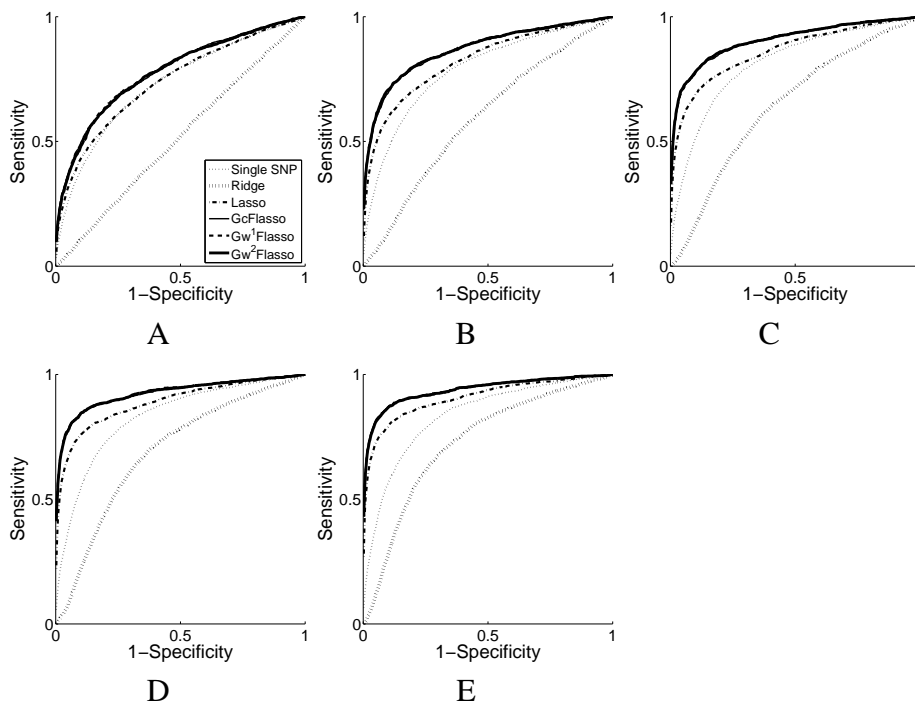


Figure 3: ROC curves for comparison of association analysis methods with different sample size N . A: $N=50$, B: $N=100$, C: $N=150$, D: $N=200$, and E: $N=250$. The effect size is 0.5, and the threshold ρ for the phenotype network is set to 0.3. Note that the curves for the G_c Flasso, G_w^1 Flasso, and G_w^2 Flasso almost entirely overlap.

3 Results

We compare the results from our proposed methods, G_c Flasso, G_w^1 Flasso and G_w^2 Flasso, with the ones from the single-marker analysis as well as multivariate regression methods such as the ridge regression and the lasso that do not use any structural information in the phenotypes. In the ridge regression, we set the regularization parameter to 0.0001, which is equivalent to adding a small value of 0.0001 to the diagonal of $\mathbf{X}'\mathbf{X}$ to make the standard regression problem non-singular. For the lasso and our proposed methods, we used the gradient-descent search for the regularization parameters λ and γ as described in Appendix. We used $(-\log(p\text{-value}))$ for the standard single-marker analysis, and the absolute value of regression coefficients $|\beta_{jk}|$'s for the multivariate regression methods and our proposed methods, as a measure of the strength of association.

3.1 Simulation Study

We evaluate the performance of the association methods based on two criteria, sensitivity/specificity and phenotype prediction error. The sensitivity and specificity measure whether the given method can successfully detect the true association SNPs with few false positives. The (1-specificity) and sensitivity are equivalent to type I error rate and (1-type II error rate), and their plot is widely known

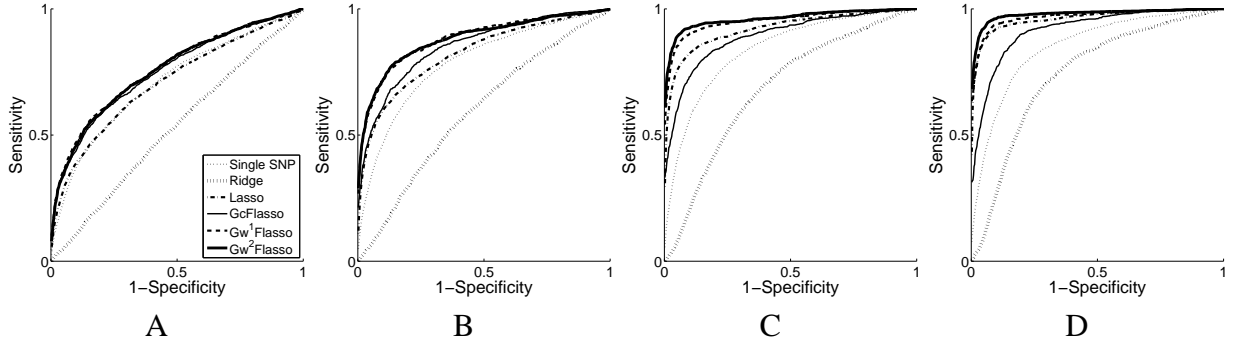


Figure 4: ROC curves for comparison of association analysis methods with varying effect size. Effect size is A: 0.3, B: 0.5, C: 0.8, and D: 1.0. The sample size is 100, and the threshold ρ for the phenotype correlation graph is 0.1.

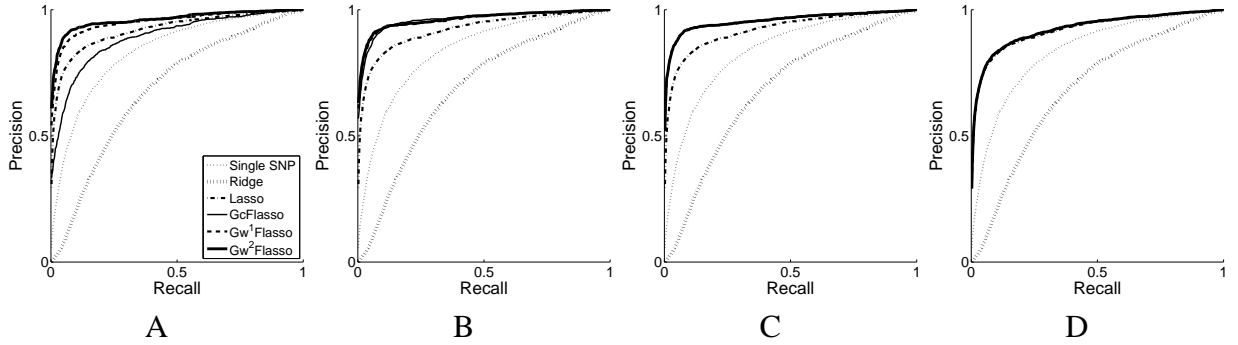


Figure 5: Precision-Recall curves for comparison of association analysis methods with different values of threshold (ρ) for the phenotype correlation network. A: $\rho=0.1$, B: $\rho=0.3$, C: $\rho=0.5$, and D: $\rho=0.7$. The sample size is 100, and the effect size is 0.8.

as a receiver operating characteristic (ROC) curve. The phenotype prediction error represents how accurately we can predict the values of phenotypes given the genotypes of new individuals, using the regression coefficients estimated from the previously available genotype and phenotype data. We generate additional dataset of 50 individuals, \mathbf{y}^{new} and \mathbf{X}^{new} , and compute the phenotype prediction error as sum of squared differences between the true values \mathbf{y}^{new} and predicted values $\hat{\mathbf{y}}^{\text{new}}$ of the phenotypes, $\sum_k (\mathbf{y}_k^{\text{new}} - \hat{\mathbf{y}}_k^{\text{new}})' \cdot (\mathbf{y}_k^{\text{new}} - \hat{\mathbf{y}}_k^{\text{new}})$, where $\hat{\mathbf{y}}_k^{\text{new}} = \mathbf{X}_k^{\text{new}} \hat{\boldsymbol{\beta}}_k$. For both criteria for measuring performance, we show results averaged over 50 randomly generated datasets.

In the results shown below, for each dataset of size N , we fit the lasso and the graph-guided methods using $(N - 30)$ samples, and use the remaining 30 samples as a validation set for determining the regularization parameters. Once we determine the regularization parameters, we use the entire dataset of size N to estimate the final regression coefficients given the selected regularization parameters.

We apply the various association methods to datasets with varying sample sizes, and show the ROC curves in Figure 3. We used the threshold $\rho=0.3$ to obtain the phenotype correlation graph, and set the effect size to 0.5. The results confirm that the lasso is an effective method for detecting

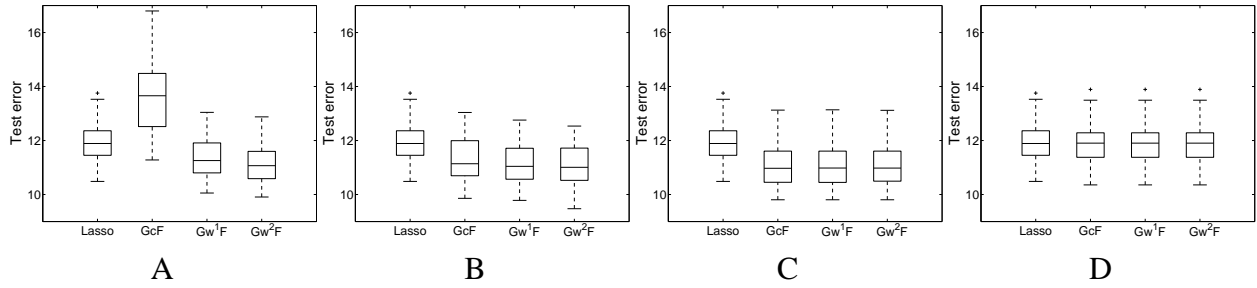


Figure 6: Comparison of association analysis methods in terms of phenotype prediction error. The threshold ρ for the phenotype correlation network is A: $\rho=0.1$, B: $\rho=0.3$, C: $\rho=0.5$, and D: $\rho=0.7$.

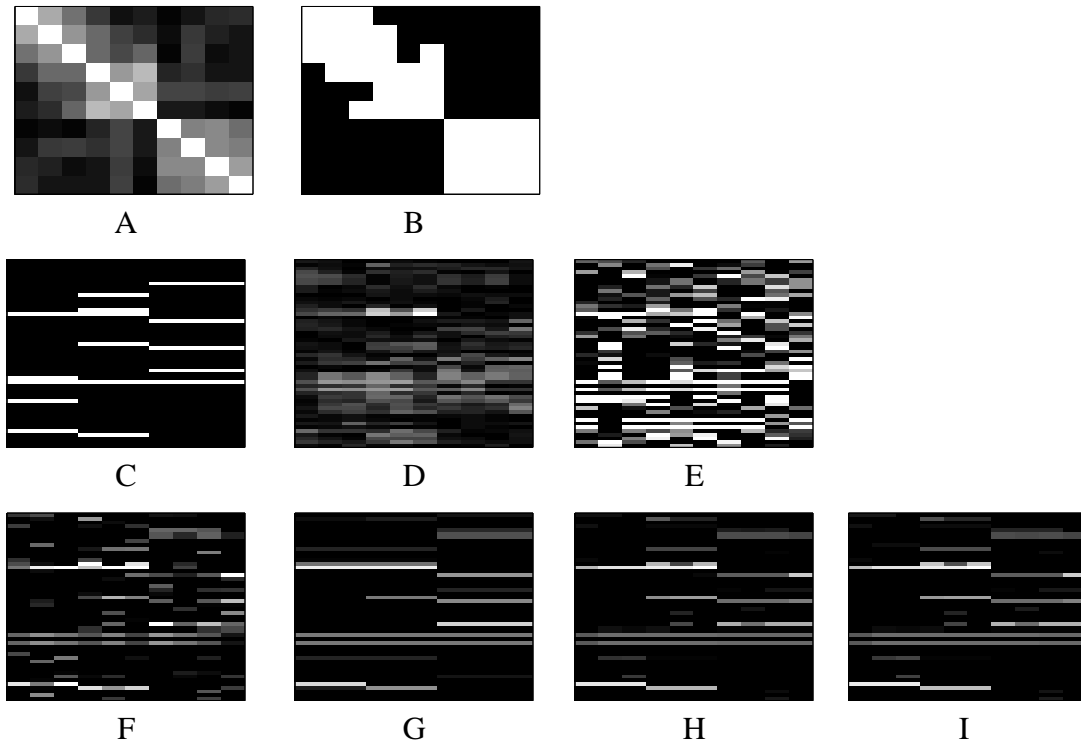


Figure 7: Results of association analysis by different methods based on a single simulated dataset. Effect size 0.8 and threshold $\rho = 0.3$ for the phenotype correlation graph are used. Bright pixels indicate large values. A: The correlation coefficient matrix of phenotypes, B: the edges of the phenotype correlation graph obtained at threshold 0.3 are shown as white pixels, C: The true regression coefficients used in simulation. Rows correspond to SNPs and columns to phenotypes. D: $-\log(p\text{-value})$. Absolute values of the estimated regression coefficients are shown for E: ridge regression, F: lasso, G: $G_c\text{Flasso}$, H: $G_w^1\text{Flasso}$, and I: $G_w^2\text{Flasso}$.

true causal SNPs and is affected less by the irrelevant SNPs, compared to the single-marker analysis and ridge regression. When we use the weighted fusion penalty in addition to the lasso penalty as in $G_c\text{Flasso}$, $G_w^1\text{Flasso}$, and $G_w^2\text{Flasso}$, the performance significantly improves over the lasso

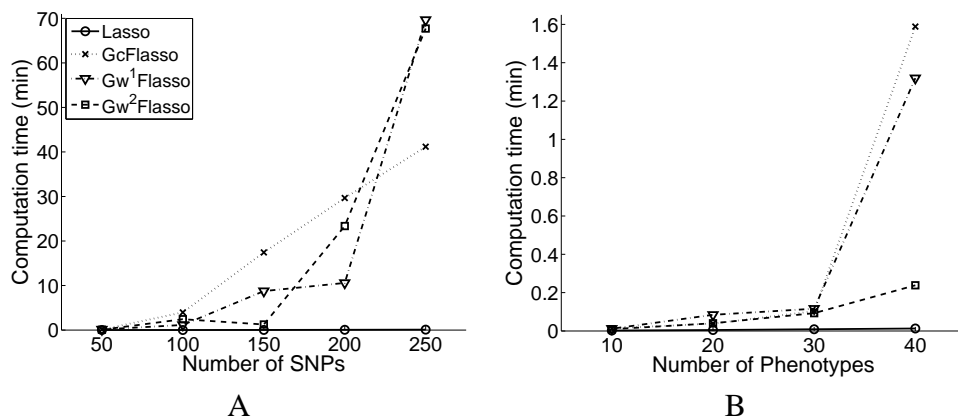


Figure 8: Comparison of the computation time for lasso, G_c Flasso, G_w^1 Flasso, and G_w^2 Flasso. A: Varying the number of SNPs with the number of phenotypes fixed at 10. The phenotype correlation graph at threshold $\rho = 0.3$ with 31 edges is used. B: Varying the number of phenotypes with the number of SNPs fixed at 50. The phenotype networks are obtained using threshold $\rho = 0.3$. The number of edges in each phenotype network is 11, 34, 53, 88, and 142 for the number of phenotypes 10, 20, 30, 40, and 50, respectively.

across all of the samples sizes shown in Figure 3.

In order to see how the effect size affects the performance of the methods for association analysis, we vary the effect size and show the ROC curves in Figure 4, for the threshold $\rho=0.1$ of the phenotype correlation network and sample size $N = 100$. The G_w^1 Flasso and G_w^2 Flasso outperform all of the other methods across all of the effect sizes. Because of the relatively low value of the threshold $\rho = 0.1$, the correlation phenotype contains many edges between a pair of phenotypes that are only weakly correlated. Thus, the G_c Flasso that does not distinguish edges for strong correlation from those for weak correlation does not show a consistent performance across different effect size, performing better than the lasso at effect size 0.3 but worse than the lasso at effect size 1.0. The G_w^1 Flasso and G_w^2 Flasso have the flexibility to handle different strengths of correlation in the graph, and consistently outperforms G_c Flasso as well as the methods that do not consider the structural information in the phenotypes.

In order to examine the effect of the threshold ρ for the phenotype correlation graph on the performance of our methods, we evaluate the GFlasso methods with ρ at 0.1, 0.3, 0.5, and 0.7, and show the ROC curves in Figure 5. We include the ROC curves for the single-marker analysis, the ridge regression, and the lasso that do not use the thresholded phenotype correlation graph in each panel of Figure 5 repeatedly for the ease of comparison. We use the sample size $N = 100$ and the effect size 0.8. Regardless of the threshold ρ , the G_w^1 Flasso and G_w^2 Flasso outperform all of the other methods or perform at least as well as the lasso. As we have seen in Figure 4, the G_c Flasso does not have the flexibility of accommodating edges of varying correlation strength in the phenotype correlation graph, and this negatively affects the performance of the G_c Flasso at the low threshold $\rho = 0.1$ in Figure 4A. As we increase the threshold ρ in Figures 4B and C, the phenotype correlation graph include only those edges with significant correlations.

Thus, the performance of $G_c\text{Flasso}$ approaches that of $G_w^1\text{Flasso}$ and $G_w^2\text{Flasso}$, and the curves of the three methods in the $G\text{Flasso}$ family almost entirely overlap. When the threshold is relatively high at $\rho = 0.7$, the number of edges in the graph is close to 0, effectively removing the fusion penalty. As a result, the performance of the graph-guided methods becomes close to the lasso. Overall, taking into account the correlation structure in phenotypes improves the detection rate of true causal SNPs. Once the phenotype correlation graph includes the edges that capture strong correlations, including more edges by further lowering the threshold ρ does not significantly affect the performance of $G_w^1\text{Flasso}$ and $G_w^2\text{Flasso}$. The same tendency is shown in the prediction errors in Figure 6.

We show an example of a simulated dataset and the estimated association strength in Figure 7, using the sample size $N = 100$ and effect size 0.8. Although the lasso is more successful in setting the regression coefficients of irrelevant SNPs to zero than the ridge regression, it still finds many SNPs as having a non-zero association strength. The $G_c\text{Flasso}$, $G_w^1\text{Flasso}$, and $G_w^2\text{Flasso}$ remove most of those spurious SNPs, and shows a clear block-structure in the estimated regression coefficients, with each causal SNP spanning subgroups of correlated phenotypes. Since $G_c\text{Flasso}$ uses only the information on the presence or absence of edges, when edges of weak correlation connect nodes across two true subgraphs, the $G_c\text{Flasso}$ is unable to ignore the weak edges, and fuses the effect of SNPs on the phenotypes across those two subgraphs. This undesirable property of $G_c\text{Flasso}$ disappears when we incorporate the edge weights in $G_w^1\text{Flasso}$ and $G_w^2\text{Flasso}$.

We show the computation time for solving a single optimization problem for the lasso, $G_c\text{Flasso}$, and $G_w\text{Flasso}$ in Figure 8 for varying number of SNPs and phenotypes.

3.2 Case Study Using Asthma Dataset

Figure 9A shows the correlation matrix of the phenotypes after reordering the phenotypes using the agglomerative hierarchical clustering algorithm so that highly correlated phenotypes are clustered with a block structure along the diagonal. Using threshold $\rho = 0.7$, we obtain a phenotype correlation graph as shown in Figure 9B, where the white pixel at position (i, j) indicates that the i -th and j -th phenotypes are connected with an edge in the graph. The graph shows several blocks of white pixels representing densely connected subgraphs. We show the full graph in Figure 1. We present results for the single-marker regression analysis, the ridge regression, the lasso, $G_c\text{Flasso}$, $G_w^1\text{Flasso}$, and $G_w^2\text{Flasso}$ in Figure 9C-H, respectively, where the rows represent phenotypes, and the columns correspond to genotypes, with bright pixels indicating high strength of association. The phenotypes in rows are rearranged according to the ordering given by the agglomerative hierarchical clustering so that each row in Figures 9C-H is aligned with the phenotypes in the correlation matrix in Figure 9A. In the fusion penalty in our proposed methods, we use the edges in Figure 9B obtained at threshold $\rho = 0.7$. The graph obtained at threshold $\rho = 0.7$ seems to capture the previously known dependencies among the clinical traits such as subnetworks corresponding to lung physiology and quality of life. We select the regularization parameters in the lasso, $G_c\text{Flasso}$, $G_w^1\text{Flasso}$, and $G_w^2\text{Flasso}$ using a five-fold cross validation.

As shown in Figures 9C and E, both the single-marker regression analysis and the lasso find a SNP near the top row, known as Q551R, as significantly associated with a block of correlated phenotypes. This subset of traits corresponds to the bottom subnetwork (consisting of baselineFEV1,

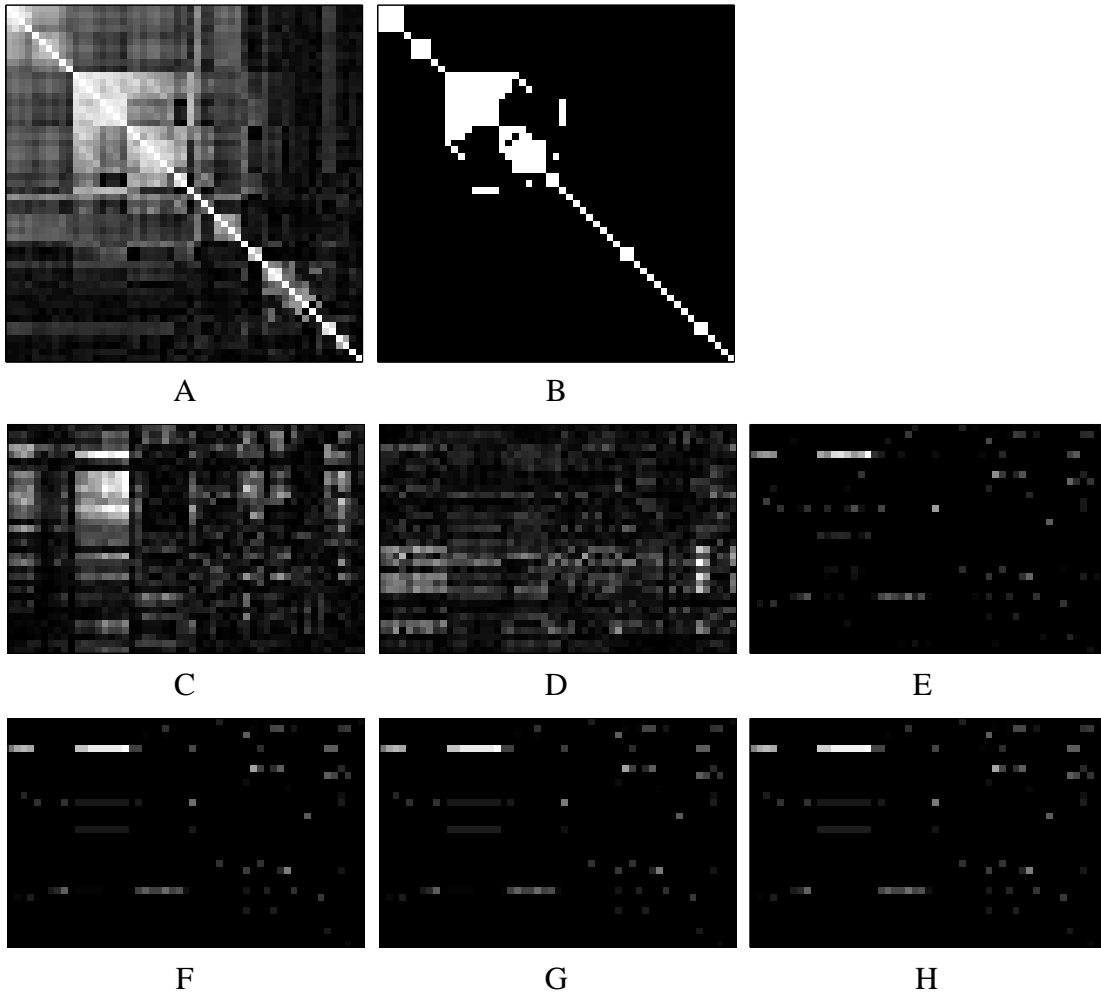


Figure 9: Results for the association analysis of the asthma dataset. A: Phenotype correlation matrix. B: Phenotype correlation matrix thresholded at $\rho = 0.7$. C: $-\log(p\text{-value})$ from single-marker statistical tests using a single-phenotype analysis. Estimated β_k 's for D: ridge regression, E: lasso, F: $G_c\text{Flasso}$, G: $G_w^1\text{Flasso}$, and H: $G_w^2\text{Flasso}$.

PreFEFPred, AvgNO, BMI, PostbroPred, BaseFEVPer, PredrugFEV1P, MaxFEV1P, FEV1Diff, and PostFEF) that resides within the large subnetwork on the left-hand side of Figure 1, and represents traits related to lung physiology. This Q551R SNP has been previously found associated with severe asthma and its traits for lung physiology [37], and our results confirm this previous finding. In addition, the results from the single-marker analysis in Figure 9C show that on the downstream of this SNP, there is a set of adjacent SNPs that appears to be in linkage disequilibrium with this SNP and at the same time has generally a high level of association with the same subset of phenotypes. On the other hand, the lasso in Figure 9E sets most of the regression coefficients for this block of SNPs in linkage disequilibrium with Q551R to zero, identifying a single SNP as significant. This confirms that the lasso is an effective method for finding sparse estimates of the regression coefficients, ignoring most of the irrelevant markers by setting corresponding re-

Table 1: Summary of results for the association analysis of the asthma dataset

ρ	Number of edges	Number of nonzero regression coefficients			
		Lasso	G_c Flasso	G_w^1 Flasso	G_w^2 Flasso
0.3	421	125	105	106	108
0.5	165		108	107	107
0.7	71		105	105	110
0.9	11		125	123	123

gression coefficients to zero. The ridge regression as shown in Figure 9D does not have the same property of encouraging sparsity as the lasso. In fact, in statistical literature, it is well-known that the ridge regression performs poorly in problems that require a selection of a small number of markers affecting phenotypes.

Since our methods in the GFlasso family include the lasso penalty, the results from G_c Flasso, G_w^1 Flasso, and G_w^2 Flasso show the same property of sparsity as the lasso in their estimates, as can be seen in Figures 9F-H. In addition, because of the fusion penalty, the regression coefficients estimated by our methods form a block structure, where the regression coefficients for each SNP are set to the same value within each block. Thus, each horizontal bar indicates a SNP influencing a correlated block of phenotypes. It is clear that the horizontal bars in Figures 9F-H are generally aligned with the blocks of highly correlated phenotypes in Figure 9A. This block structure is much weaker in the results from the lasso in Figure 9E. For example, Figures 9F-H show that the SNPs rs3024660 and rs3024622 on the downstream of Q551R are associated with the same block of traits as Q551R, generating an interesting new hypothesis that these two SNPs as well as Q551R might be jointly associated with the same subset of clinical traits. This block structure shared by the two SNPs is not obvious in the results of single-marker tests and the lasso.

We fit the lasso and our methods in the GFlasso family, while varying the threshold for the correlation graph, and summarize the results in Table 1. When the threshold is high at $\rho = 0.9$, only a very small number of edges are included in the phenotype correlation graph, and the contribution of the graph-guided fusion penalty in GFlasso is low. Thus, the number of non-zero regression coefficients found by the G_c Flasso, G_w^1 Flasso, and G_w^2 Flasso is similar to the result of the lasso that does not have the fusion penalty. When we lower the threshold to $\rho = 0.7$, the number of non-zero regression coefficients decreases significantly for our methods. As can be seen in Figure 9B, most of the significant correlation structure is captured in the thresholded correlation graph at $\rho = 0.7$. Thus, as we further lower the threshold, the number of non-zero regression coefficients generally remains unchanged.

4 Discussion

When multiple phenotypes are involved in association mapping, it is important to combine the information across phenotypes and make use of the full information available in data in order to achieve the maximum power. Most of the previous approaches either considered each phenotype separately, or used a two-stage method that first extracts relatively primitive types of phenotype correlation structure such as phenotypes transformed through PCA or subgroups of phenotypes found by clustering algorithms, and then performs a single-phenotype analysis in the second stage. Networks or graphs have been extensively studied as a representation of correlation structure of phenotypes such as gene expression or clinical traits because they provide a flexible and explicit form of representation for capturing dependencies. Graphs contain rich information on phenotype interaction patterns such as densely connected subgraphs that can be interpreted as a cluster of phenotypes participating in the same biological process. Applying a clustering algorithm to identify subgraphs as in the two-stage methods can potentially result in a loss of information, decreasing the power of the study. Developing a tool for multiple-phenotype association mapping that can directly leverage this full graph structure of phenotypes can offer a way to combine the large body of previous research in network analysis with the work on association mapping.

In this article, we proposed a new family of regression methods called GFlasso that directly incorporates the correlation structure represented as a graph and uses this information to guide the estimation process. The methods consider all of the phenotypes jointly and estimates the model in a single statistical framework instead of using a two-stage algorithm. Often, we are interested in detecting genetic variations that perturb a sub-module of phenotypes rather than a single phenotype, and the GFlasso achieves this through fusion penalty in addition to the lasso penalty that encourages parsimony in the estimated model. The fusion penalty locally fuses two regression coefficients for a pair of correlated phenotypes, and this effect propagates through edges of graphs, effectively applying fusion to all of the nodes within each subgraph. The G_c Flasso used an unweighted graph structure as a guide to find a subset of relevant covariates that jointly affect highly correlated outputs. The G_w Flasso used additional information of edge weights to further add flexibility. Using simulated and asthma datasets, we demonstrated that including richer information on phenotype structure as in the G_w Flasso and G_c Flasso improves the accuracy in detecting true associations.

We used a simple scheme of a thresholded correlation graph for learning the correlation structure for phenotypes to be used in the GFlasso. Many different types of network-learning algorithms have been developed previously. For example, graphical Gaussian models (GGMs) are constructed based on partial correlations that capture the direct influence of interacting nodes, and have been commonly used for inferring gene networks from microarray data. Furthermore, in order to handle the case with a large number of nodes and a relatively small sample size, sparse GGMs have been developed. It would be interesting to see if using more sophisticated graph learning algorithms can improve the performance of the GFlasso.

In this study, we assumed that the graph structure is available from pre-processing step. One of the possible extensions of the proposed method is to learn the graph structure and the regression coefficients jointly by combining the GFlasso with the graphical lasso [39] that learns sparse covariance matrix for phenotypes. In *Geronemo*, both the module network structure and the markers

of regulators regulating modules were learned simultaneously, although the genotype information was limited to the markers within regulators [23]. When the GFlasso is extended to learn the graph structure as well as regression coefficients, the method can be applied to a full genome-wide scan for associations.

The GFlasso considered only dependencies among phenotypes, and did not assume any dependencies among the markers. Since recombination breaks chromosomes during meiosis at non-random sites, segments of chromosomes are inherited as a unit from ancestors to descendants rather than an individual nucleotide, creating a relatively low diversity in observed haplotypes than would be expected if each allele were inherited independently. Thus, SNPs with high linkage disequilibrium are likely to contribute jointly to a phenotype in a regression-based penetrance function. By incorporating the structural information in both the genome and phenome, we expect to be able to identify a block of correlated markers influencing a set of correlated phenotypes.

Appendix: Parameter Estimation

In this section, we describe the procedure for obtaining estimates of the regression coefficients in G_w Flasso. Since the G_c Flasso is a special case of G_w Flasso with $f(r) = 1$, the same procedure can be applied to G_c Flasso in a straight-forward manner. The optimization problem in Equation (5) is the Lagrangian form of the following optimization problem:

$$\begin{aligned} G_w\text{Flasso : } \quad & \hat{\mathbf{B}}^{\text{GW}} = \operatorname{argmin} \sum_k (\mathbf{y}_k - \mathbf{X}\boldsymbol{\beta}_k)^T \cdot (\mathbf{y}_k - \mathbf{X}\boldsymbol{\beta}_k) \\ & \text{s. t. } \quad \sum_k \sum_j |\beta_{jk}| \leq s_1 \text{ and } \sum_{(m,l) \in E} f(r_{ml}) \sum_j |\beta_{jm} - \operatorname{sign}(r_{ml})\beta_{jl}| \leq s_2. \end{aligned} \quad (6)$$

where s_1 and s_2 are tuning parameters corresponding to λ and γ in Equation (5).

Since the objective function and constraints in Equation (6) are convex, we can formulate this problem as a quadratic programming (QP) as follows. Let $\boldsymbol{\beta}_c$ denote a $(J \cdot K)$ -vector that can be obtained by concatenating $\boldsymbol{\beta}_k$'s such that $\boldsymbol{\beta}_c = (\boldsymbol{\beta}_1^T, \dots, \boldsymbol{\beta}_K^T)^T$. We represent $\beta_{jk} = \beta_{jk}^+ - \beta_{jk}^-$, where $\beta_{jk}^+ \geq 0$ and $\beta_{jk}^- \geq 0$, and let $\boldsymbol{\beta}_c^+$ and $\boldsymbol{\beta}_c^-$ denote $(J \cdot K)$ -vectors of β_{jk}^+ 's and β_{jk}^- 's respectively. We define $\theta_{j,(m,l)} = \beta_{j,m} - \operatorname{sign}(r_{ml})\beta_{j,l}$ for all $(m,l) \in E$ and $j = 1, \dots, J$, and let $\theta_{j,(m,l)} = \theta_{j,(m,l)}^+ - \theta_{j,(m,l)}^-$ with $\theta_{j,(m,l)}^+ \geq 0$ and $\theta_{j,(m,l)}^- \geq 0$. Let $\boldsymbol{\theta}_c = (\boldsymbol{\theta}_1^T, \dots, \boldsymbol{\theta}_{|E|}^T)^T$, where $\boldsymbol{\theta}_e = (\theta_{1,e}, \dots, \theta_{J,e})^T$ for $e = (m,l) \in E$. We define $\boldsymbol{\theta}_c^+$ and $\boldsymbol{\theta}_c^-$ similarly. Let M be a $(J \cdot |E|) \times (J \cdot K)$ matrix, or equivalently a $|E| \times K$ matrix of $J \times J$ sub-matrices. Each sub-matrix $\mathbf{B}_{e,k}$ of M for $e = 1, \dots, |E|$ and $k = 1, \dots, K$ is an identity matrix if $e = (m,l)$ and $k = m$. If $e = (m,l)$ and $k = l$, $\mathbf{B}_{e,k}$ is set to a diagonal matrix with -1 along the diagonal. Otherwise, $\mathbf{B}_{e,k}$ is set to a matrix of 0's. Let R be a $(J \cdot |E|)$ -vector of $|E|$ sub-vectors with length J . Each sub-vector in R is set to $f(r_{m,l}) \cdot \mathbf{1}_J$, where $\mathbf{1}_J$ represents a J -vector of 1's. Then, the QP problem for Equation (6) can be written as

$$\min \sum_k (\mathbf{y}_k - \mathbf{X}\boldsymbol{\beta}_k)^T \cdot (\mathbf{y}_k - \mathbf{X}\boldsymbol{\beta}_k) \quad (7)$$

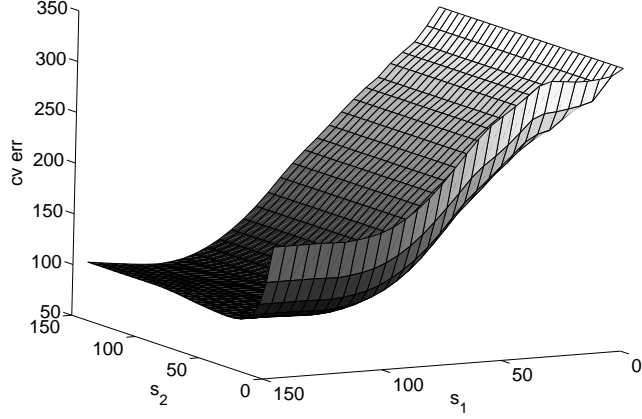


Figure 10: An example of the cross validation error surface over a grid of (s_1, s_2) from graph-weighted fused lasso.

subject to

$$\begin{pmatrix} 0 \\ 0 \\ 0 \\ 0 \end{pmatrix} \leq \begin{pmatrix} I & -I & I & 0 & 0 \\ M & 0 & 0 & -I & I \\ 0 & \mathbf{1}_{(J \cdot K)}^T & \mathbf{1}_{(J \cdot K)}^T & 0 & 0 \\ 0 & 0 & 0 & R^T & R^T \end{pmatrix} \begin{pmatrix} \beta_c \\ \beta_c^+ \\ \beta_c^- \\ \theta_c^+ \\ \theta_c^- \end{pmatrix} \leq \begin{pmatrix} 0 \\ 0 \\ s_1 \\ s_2 \end{pmatrix}, \quad (8)$$

where I is a $(J \cdot K) \times (J \cdot K)$ identity matrix, and $\mathbf{1}_{(J \cdot K)}$ is a $(J \cdot K)$ -vector of 1's.

The above QP procedure finds the optimal β_k 's for fixed s_1 and s_2 . The s_1 and s_2 can be selected via cross-validation by running the QP procedure on a grid of s_1 and s_2 and selecting the s_1 and s_2 that give the lowest validation-set error $C(s_1, s_2)$ as was suggested for the fused lasso [35]. The QP solver for G_w Flasso runs reasonably fast for fixed s_1 and s_2 , but the grid search with a cross-validation can be time-consuming. Instead, we take a gradient-descent approach that iterates between solving the QP with the current values of s_1 and s_2 and updating s_1 and s_2 with $(s_1, s_2) \leftarrow (s_1, s_2) - \eta \nabla C(s_1, s_2)$, where the gradient is approximated by a finite difference vector $(\frac{C(s_1+h, s_2) - C(s_1, s_2)}{h}, \frac{C(s_1, s_2+h) - C(s_1, s_2)}{h})$. Figure 10 shows a typical example of the cross-validation error over the grid of (s_1, s_2) from G_w Flasso. We exploit the shape of this error surface, and determine the initial values $s_1^{(0)}$ and $s_2^{(0)}$ for the gradient descent as follows. We first search for $s_1^{(0)}$ that produces the minimum cross-validation error by solving the lasso with $s_2 = \infty$. Then we fix s_1 at $s_1^{(0)}$, and perform another one-dimensional search in the direction of s_2 , starting from 0 to find the optimal $s_2^{(0)}$ for the G_w Flasso along this path. In our experiments, we found that the initial values obtained by this procedure was sufficiently close to the global optimum, and that it converged to the optimum within a relatively small number of iterations.

Acknowledgments

This material is based upon work supported by an NSF CAREER Award to EPX under grant No. DBI-0546594, and NSF grants CCF-0523757 and DBI-0640543. EPX is also supported by an Alfred P. Sloan Research Fellowship of Computer Science. We thank Sally Winzel, M.D. for providing the SARP dataset, and for her helpful discussions on the Asthma association study.

Web Resources

- HapMap project: <http://www.hapmap.org>
- Software for GFlasso: <http://www.cs.cmu.edu/~sssykim/gflasso.html>

References

- [1] The International HapMap Consortium. (2005). A haplotype map of the human genome. *Nature* 437, 1399–1320.
- [2] Wellcome Trust Case Control Consortium. (2007). Genome-wide association study of 14,000 cases of seven common diseases and 3,000 shared controls. *Nature* 447, 661–78.
- [3] Li, Y., Sung, W., and Liu, J. (2007). Association mapping via regularized regression analysis of single-nucleotide-polymorphism haplotypes in variable-sized sliding windows. *American Journal of Human Genetics* 80, 705–715.
- [4] Servin, B. and Stephens, M. (2007). Imputation-based analysis of association studies: candidate regions and quantitative traits. *PLoS Genetics* 3, 1296–1308.
- [5] Malo, N., Libiger, O., and Schork, N. (2008). Accommodating linkage disequilibrium in genetic-association analyses via ridge regression. *American Journal of Human Genetics* 82, 375–85.
- [6] Moore, W., Bleecker, E., Curran-Everett, D., Erzurum, S., Ameredes, B., Bacharier, L., Calhoun, W., Castro, M., Chung, K., and Clark, M. (2007). Characterization of the severe asthma phenotype by the National Heart, Lung, and Blood Institute’s Severe Asthma Research Program. *Journal of Allergy and Clinical Immunology* 119, 405–13.
- [7] Butte, A. and Kohane, I. (2006). Creation and implications of a phenome-genome network. *Nature Biotechnology* 24, 55–62.
- [8] Mehan, M., Nunez-Iglesias, J., Kalakrishnan, M., Waterman, M., and Zhou, X. (2008). An integrative network approach to map the transcriptome to the phenome. In *Proceedings of the conference on research in computational molecular biology* pp. 232–45.
- [9] Toh, H. and Horimoto, K. (2002). Inference of a genetic network by a combined approach of cluster analysis and graphical gaussian modeling. *Bioinformatics* 18, 287–97.

- [10] Friedman, N. (2004). Inferring cellular networks using probabilistic graphical models. *Science* 303, 799–805.
- [11] Segal, E., Shapira, M., Regev, A., Pe’er, D., Botstein, D., Koller, D., and Friedman, N. (2003). Module networks: identifying regulatory modules and their condition-specific regulators from gene expression data. *Nature Genetics* 34, 166–78.
- [12] Wille, A., Zimmermann, P., Vranova, E., Furholz, A., Laule, O., Bleuler, S., Hennig, A., Preli, A., von Rohr, P., Thiele, L., et al. (2004). Sparse graphical gaussian modeling of the isoprenoid gene network in *arabidopsis thaliana*. *Genome Biology* 5, R92.
- [13] Schafer, J. and Strimmer, K. (2005). An empirical Bayes approach to inferring large-scale gene association networks. *Bioinformatics* 21, 754–64.
- [14] Basso, K., Margolin, A., Stolovitzky, G., Klein, U., Dalla-Favera, R., and Califano, A. (2005). Reverse engineering of regulatory networks in human B cells. *Nature Genetics* 37, 382–90.
- [15] Hu, H., Yan, X., Huang, Y., Han, J., and Zhou, X. (2005). Mining coherent dense subgraphs across massive biological networks for functional discovery. *Bioinformatics* 21, 213–221.
- [16] Stranger, B., Forrest, M., Clark, A., Minichiello, M., Deutsch, S., Lyle, R., Hunt, S., Kahl, B., Antonarakis, S., Tavare, S., et al. (2005). Genome-wide associations of gene expression variation in humans. *PLoS Genetics* 1, 695–704.
- [17] Cheung, V., Spielman, R., Ewens, K., Weber, T., Morley, M., and Burdick, J. (2005). Mapping determinants of human gene expression by regional and genome-wide association. *Nature* 437, 1365–1369.
- [18] Knott, S. and Haley, C. (2000). Multitrait least squares for quantitative trait loci detection. *Genetics* 156, 899–911.
- [19] Xu, C., Li, Z., and Xu, S. (2005). Joint mapping of quantitative trait loci for multiple binary characters. *Genetics* 169, 1045–59.
- [20] Liu, J., Liu, Y., Liu, X., and Deng, H. (2007). Bayesian mapping of quantitative trait loci for multiple complex traits with the use of variance components. *The American Journal of Human Genetics* 81, 304–20.
- [21] Weller, J., Wiggans, G., Vanraden, P., and Ron, M. (1996). Application of a canonical transformation to detection of quantitative trait loci with the aid of genetic markers in a multi-trait experiment. *Theoretical and Applied Genetics* 92, 998–1002.
- [22] Mangin, B., Thoquet, B., and Grimsley, N. (1998). Pleiotropic QTL analysis. *Biometrics* 54, 89–99.
- [23] Lee, S.-I., Pe’er, D., Dudley, A., Church, G., and Koller, D. (2006). Identifying regulatory mechanisms using individual variation reveals key role for chromatin modification. *PNAS* 103, 14062–67.

- [24] Chen, Y., Zhu, J., Lum, P., Yang, X., Pinto, S., MacNeil, D., Zhang, C., Lamb, J., Edwards, S., Sieberts, S., et al. (2008). Variations in DNA elucidate molecular networks that cause disease. *Nature* 452, 429–35.
- [25] Emilsson, V., Thorleifsson, G., Zhang, B., Leonardson, A., Zink, F., Zhu, J., Carlson, S., Helgason, A., Walters, G., Gunnarsdottir, S., et al. (2008). Variations in dna elucidate molecular networks that cause disease. *Nature* 452, 423–28.
- [26] Zhu, J., Zhang, B., Smith, E., Drees, B., Brem, R., Kruglyak, L., Bumgarner, R., and Schadt, E. (2008). Integrating large-scale functional genomic data to dissect the complexity of yeast regulatory networks. *Nature Genetics* 40, 854–61.
- [27] Tibshirani, R. (1996). Regression shrinkage and selection via the lasso. *Journal of Royal Statistical Society, Series B* 58, 267–288.
- [28] Zhao, P. and Yu, B. (2006). On model selection consistency of lasso. *Journal of Machine Learning Research* 7(Nov), 2541–2563.
- [29] Weisberg, S. (1980). *Applied Linear Regression*. (Wiley, New York).
- [30] Hoerl, A., Kennard, R., and Baldwin, K. (1975). Ridge regression: Some simulations. *Communications in Statistics - Theory and Methods* 4, 105–23.
- [31] Efron, B., Hastie, T., and Johnstone, R., I. Tibshirani. (2004). Least angle regression. *Annals of Statistics* 32, 407–499.
- [32] Butte, A., Tamayo, P., Slonim, D., Golub, T., and Kohane, I. (2000). Discovering functional relationships between RNA expression and chemotherapeutic susceptibility using relevance networks. *Proc. Natl Acad. Sci., USA* 97, 12182–86.
- [33] Carter, S., Brechbuhler, C., Griffin, M., and Bond, A. (2004). Gene co-expression network topology provides a framework for molecular characterization of cellular state. *Bioinformatics* 20, 2242–50.
- [34] Zhang, B. and Horvath, S. (2005). A general framework for weighted gene co-expression network analysis. *Statistical Applications in Genetics and Molecular Biology* 4, Article 17.
- [35] Tibshirani, R., Saunders, M., Rosset, S., Zhu, J., and Knight, K. (2005). Sparsity and smoothness via the fused lasso. *Journal of Royal Statistical Society, Series B* 67, 91–108.
- [36] Knight, K. and Fu, W. (2000). Asymptotics for lasso-type estimators. *The Annals of Statistics* 28, 1356–1378.
- [37] Wenzel, S., Balzar, S., Ampleford, E., Hawkins, G., Busse, W., Calhoun, W., Castro, M., Chung, K. F., Erzurum, S., Gaston, B., et al. (2007). IL4R α mutations are associated with asthma exacerbations and mast cell/IgE expression. *American Journal of Respiratory and Critical Care Medicine* 175, 570–76.

- [38] Li, N. and Stephens, M. (2003). Modelling linkage disequilibrium, and identifying recombination hotspots using snp data. *Genetics* 165, 2213–2233.
- [39] Friedman, T., J. Hastie and Tibshirani, R. (2008). Sparse inverse covariance estimation with the graphical lasso. *Biostatistics* 9, 432–441.